RESEARCH PAPER
Contrib. Sci. & Tech Eng, 2024, 1(2)
Homepage: https://cste.journals.umz.ac.ir/
DOI: 10.22080/cste.2024.5091

Comparison of SIED and Canny Algorithm in Caspian Sea Surface Temperature Front Detection Using Satellite Image

Shahnaz Kaleji [1], Mohammad Akbarinasab [2], Abbas Einali [2*]

[1] *Faculty of Environmental and Marine Sciences, University of Mazandaran, Babolsar, Iran.*

[2] *Faculty of Environmental and Marine Sciences, University of Mazandaran, Babolsar, Iran.*

Article Info
Received 10 April 2024
Accepted 10 May 2024
Available online 1 June 2024

Keywords:
Surface Temperature Front;
SIED Method;
Canny Algorithm;
MODIS;
Caspian Sea.

Abstract:
Sea surface temperature fronts, narrow strips on the ocean's surface with significant temperature changes, play a crucial role in marine ecosystems and climate regulation. This study compares the Single Images Edge Detection (SIED) and Canny algorithms in detecting sea surface temperature fronts in the Caspian Sea using MODIS satellite images from 2015 to 2019. The SIED algorithm, a population-based method, identified fronts by statistically analyzing temperature histograms within a 32×32-pixel window. In contrast, the Canny algorithm, a gradient-based method, detected fronts by calculating temperature gradients at each pixel. Both algorithms revealed seasonal and spatial variations in temperature fronts, with the highest presence of fronts detected during the winter months. The SIED algorithm found the lowest presence of stable fronts in the northern Caspian in September and April and the southern Caspian in November, March, and April. The Canny algorithm showed the lowest presence in June, March, and August. SIED detected the highest presence of stable fronts in November and December in the northern Caspian Sea and in January in the southern Caspian Sea. The Canny algorithm identified the highest presence during the first three months of the winter monsoon. Both algorithms consistently detected fronts along the eastern coasts of the Middle and South Caspian, with significant fronts near the Garabogazköl Basin and Turkmenbashi Gulf. Despite differences in detection, both methods revealed similar general patterns of temperature fronts.

***Corresponding Author:** a.einali84@umz.ac.ir.

Supplementary information: Supplementary information for this article is available at https://cste.journals.umz.ac.ir/

Please cite this paper as: Kaleji, S., Akbarinasab, M., & Einali, A. (2024). Comparison of SIED and Canny Algorithm in Caspian Sea Surface Temperature Front Detection Using Satellite Image. Contributions of Science and Technology for Engineering, 1(2), 9-18. doi: 10.22080/cste.2024.5091.

1. Introduction

A temperature front is a narrow strip on the ocean's surface where significant changes in surface temperature occur [1]. These fronts separate two bodies of water with different temperatures [2]. Recent studies indicate that ocean surface temperature fronts impact Earth's climate by influencing the stability of the atmospheric boundary layer, pressure fields, and atmospheric baroclinicity [3]. Additionally, these fronts trap suspended sediments and nutrients, creating an ideal environment for phytoplankton growth. Consequently, these areas are biodiversity hotspots [4].

Various physical processes in the oceans create different types of fronts, such as those formed by river water entering the sea [2], merging tidal currents [5], coastal and open sea upwelling [6], boundary currents [7, 8], and bathymetry [9]. Detecting temperature fronts is crucial for marine sciences, as they are critical indicators for meteorological studies, sea-atmosphere interactions, and marine ecosystems. These fronts also support biological productivity, attracting fish, birds, and marine mammals, which is essential for fisheries and biology. Understanding temperature fronts is essential for studying marine ecosystems and sea hydrodynamics [2].

The Caspian Sea, the world's largest enclosed water body, spans approximately 1160 km from north to south. It is divided into three parts: North Caspian, Middle Caspian, and South Caspian, based on its physical and geographical conditions. Global warming and human activities, such as indiscriminate river harvesting, have significantly altered the Caspian Sea's hydrodynamic regime and climate [10, 11]. These long-term changes highlight the need to monitor the Caspian Sea's oceanographic features, including temperature fronts. Without field measurement data, satellite data is a valuable alternative [11].

Remote sensing has become an efficient, cost-effective, and accessible tool for marine studies, providing valuable long-term data. One of the most critical marine parameters measured by remote sensing is ocean surface temperature, which is crucial for understanding climate change and Earth's ecosystem. Various sensors, such as the MODIS sensor on NASA's Aqua satellite, measure water

*ISSN **3060-6578***

temperature at the ocean's surface and are excellent for detecting sea surface temperature fronts [12].

Algorithms for detecting temperature fronts are generally categorized into population-based and gradient-based methods. The population-based algorithm identifies a front as a line separating two or more clusters within a region, typically spanning 16 pixels in each direction. In contrast, the gradient-based method uses changes in the gradient over a smaller range (1 to 3 pixels) to detect fronts. The SIED method, which is based on the population-based algorithm, identifies and extracts temperature fronts by statistically analyzing the histogram of water surface temperature values within a 32×32-pixel window. This method compares the average water surface temperature in different regions to identify two distinct water masses. The coherence between these masses is then checked to confirm the presence of a front, indicating two separate water bodies on either side [13].

One of the gradient-based algorithms for detecting fronts is the Canny algorithm. These algorithms calculate the gradient of sea surface temperature (SST) data, highlighting areas with significant temperature changes. The gradient magnitude is computed at each pixel, and regions with high gradient values are identified as potential fronts. This method effectively detects thermal fronts associated with various oceanographic phenomena such as upwelling, eddies, and boundary currents [14].

Kostianoy et al. [11] utilized remote sensing to study the seasonal and annual changes in the water surface temperature of the Caspian Sea, focusing on the North, South, and Middle Caspian regions, as well as the Garabogazköl Basin. The study revealed an average annual water temperature increase in the Middle and South Caspian regions across all seasons. From 1982 to 2015, the warming rates were 0.05°C and 0.04°C per year for the Middle and South Caspian, respectively, significantly higher than the previous twenty-year period's rate of 0.01°C per year. Despite the challenges posed by freezing the North Caspian Sea, similar warming trends are inferred due to temperature correlations across the Caspian Sea. This warming is attributed to global climate change. The study also explored other features observable via remote sensing, such as the temperature fronts in the Caspian Sea, particularly during the cold season. Mesoscale eddies in the Middle Caspian Sea, influenced by the warm waters from the South Caspian, move northward during the cold period. Conversely, southward currents spread cold, fresh waters from the North Caspian to the Middle Caspian. These interactions create temperature fronts in the Middle Caspian. Upwelling, another phenomenon affecting temperature fronts, varies between the western and eastern parts of the Caspian Sea. Satellite images show that upwelling is influenced by factors like depth, coastline features, prevailing winds, and current directions, as well as seasonal thermoclines, water mixing, and local eddies [11].

The SIED algorithm, developed by Cayula and Cornillon [15], was initially designed to identify fronts in sea surface temperature (SST) images and was first applied to study the Gulf Stream using AVHRR and NOAA-7 satellite images [15]. This algorithm has since been utilized in studies involving various sensors, including the NOAA sensor [16], the AVHRR Pathfinder sensor [1], and the Terra and Aqua sensors from the MODIS satellite [17]. Nieto et al. [18] evaluated different methods for detecting fronts in satellite images and highlighted the advantages of the SIED algorithm, particularly its superior detection of weaker temperature fronts [18]. Using SST data from the AVHRR satellite, Ullman and Cornillon [16] compared the SIED algorithm with MIED and gradient methods. Their findings indicated that the SIED algorithm was more efficient regarding error rate and success in identifying fronts [16]. The SIED algorithm's use of a variable-sized window enhances its adaptability to coastlines, making it an excellent choice for extracting temperature fronts in coastal areas. This adaptability is key to its effectiveness and widespread application in various remote sensing studies [19].

Ren et al. [20] developed a gradient-based algorithm to identify sea surface temperature (SST) fronts within the high-resolution South China Sea Operational Forecasting System (SCSOFS). This algorithm enhances the Canny edge detection method with post-processing to extract primary ocean fronts accurately. The study revealed that most fronts are situated near the coast, extending from the Taiwan Strait to the coasts of Vietnam, with strong seasonal signals influencing their variability [20]. Karami et al. [21] conducted a study titled "Detection of the Coastal Temperature Fronts of the Persian Gulf and the Sea of Oman Using MODIS Images." Their research demonstrated that most temperature fronts formed in dynamic regions aligned with ocean currents. They identified five stable temperature front areas far from the coast and eight near the coast. Additionally, the study determined the times of the year with the highest and lowest presence of temperature fronts in these waters [21].

The present study focused on extracting and comparing the temperature fronts of the Caspian Sea across its northern, middle, and southern regions. Applying the SIED and CANNY algorithms to five years of MODIS satellite images, the fronts were extracted and analyzed spatially and temporally. Finally, the fronts extracted by SIED and Canny methods were compared.

2. Material and methods

The current research focuses on the Caspian Sea, between latitudes 37-47°N and longitudes 47-55°E. Covering an area of 436,400 square kilometers, the Caspian Sea is the largest lake in the world. Five countries—Iran, Azerbaijan, Russia, Kazakhstan, and Turkmenistan—have access to the Caspian Sea [10]. Figure 1 illustrates the location of the Caspian Sea and its bordering countries and bathymetric contour.

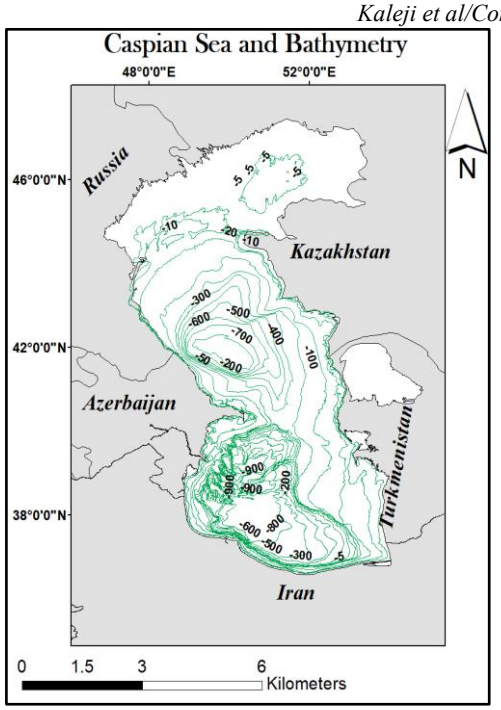

Figure 1. Location of the study area (Caspian Sea)

This study utilized images from the MODIS sensor, renowned for measuring ocean surface temperatures. The sensor's spectral range spans 0.4-14.4 µm, making it highly valuable for environmental science applications. MODIS offers spatial resolutions of 250 meters for bands 1 and 2, 500 meters for bands 3 to 7, and 1000 meters for the remaining 29 bands. Its imaging width of 2330 km allows for global coverage within 1-2 days. Key features include 12-bit radiometric sensitivity, 36 spectral bands, and advanced geometric correction. The presence of multiple thermal bands makes MODIS ideal for studying temperature fronts [22]. The Caspian Sea's surface temperature was analyzed monthly from 2015 to 2019, identifying temperature fronts using the SIED and Canny methods. In addition to spatial surveys, the temporal analysis involved comparing images from three periods each year.

The SIED algorithm employs statistical analysis of temperature distribution (water surface temperature histogram) to identify different water masses and their boundaries, known as temperature fronts. 32 x 32 pixels moving window scans the image, detecting bimodal temperature distributions. When a bimodal distribution is found, the average temperatures of the two water masses are calculated and compared to a predefined threshold. A front is confirmed if the temperature difference exceeds the threshold; otherwise, the window moves to the next section. The threshold value varies based on window size and image noise level, optimized to reduce false and missed detections [23].

The SIED algorithm involves several steps: 1) Filtering out cloudy or invalid pixels using a cloud filtering algorithm, 2) Applying a median filter with a 3x3 moving window to remove noise, 3) Using a histogram algorithm to detect bimodal distributions within a 32x32 moving window in 16 steps, 4) Applying a spatial correlation algorithm to determine if two populations are spatially separated, 5) Identifying front pixels in windows where water masses are sufficiently separated, and 6) Using a counter-following algorithm to extend recognized fronts to adjacent pixels with similar conditions [24]. The SIED algorithm, developed by Cayula and Cornillon [15], operates in three main stages: image, window, and pixel. The image stage is influenced by cloud cover. In the window stage, histogram analysis is conducted on square windows, and the resulting data is used in the pixel stage to identify front pixels through minimization. Initially, the algorithm assesses whether each window contains a single mass or body. If masses are detected, a threshold is chosen to separate these bodies [15].

When a binomial distribution is identified within a window, a correlation algorithm is employed to verify if the pixels of the two clusters are adequately separated. This correlation coefficient is utilized in two phases: first, for a single water mass, and second, for the correlation between two adjacent water masses. The correlation coefficient for the water mass W1 is calculated as C1=R1⁄T1, where (R1) represents the total correlation value between the central pixel of W1 and its neighboring pixels, and (T1) is the total correlation value within W1. The optimal correlation coefficients are dependent on the histogram window size. The minimum correlation between two water masses, W1 and W2, is calculated as C=(R1+R2)⁄(T1+T2). For a 32×32 histogram window, Cayula and Cornillon [15] determined this value to be 0.92. This calculation is crucial for distinguishing between different water masses in satellite imagery [15, 25].

The Canny algorithm is a method for detecting edges and analyzing their features based on differentiation, which is particularly useful in coastal areas [26]. This algorithm is susceptible to image noise, necessitating noise removal from the initial image before edge extraction. Typically, a simple mask or Gaussian filter is used for this purpose. The mask size (Gaussian width) affects edge detection accuracy, requiring an appropriate size selection. A threshold (T), a real number between zero and one, is considered, and for points with Gaussian values less than (T), the equation $T = \exp(X^2(2 \times \sigma^2))$ is applied. The smoothing degree is determined by sigma [20, 27, 28].

After noise removal, edge strength (gradient) can be obtained using the Sobel algorithm in both X and Y directions. For each block, the gradient magnitude is calculated using the formula $|G| = \sqrt{G_x^2 + G_y^2}$, where the magnitude (G) indicates edge strength [20, 27]. The edge direction for each block is determined using the formula $\theta = Tan^{-1}(G_x/G_y)$. Only angles of 0, 45, 90, and 135 degrees are considered edge directions.

To prevent errors, two thresholds, high (T2) and low (T1), are used for edge detection. Pixels with values less than T1 are not considered edges, while those with values greater than T2 are considered edges. If a pixel's value is between T1 and T2, it can be viewed as an edge under specific conditions, such as connectivity to edge pixels [20, 28].

This study leveraged the practical capabilities of the Canny and SIED algorithms to analyze MODIS sensor images over

a five-year period (2015-2019). Both algorithms were applied to extract temperature fronts in the Caspian Sea. A primary objective of this research was to compare the results obtained from the Canny and SIED methods. The temperature fronts were extracted and analyzed on a monthly basis, providing insights into the temporal variations and patterns in the Caspian Sea.

3. Result

This section presents the monthly temperature fronts obtained from satellite images using the SIED and Canny algorithms. These temperature fronts are categorized into three distinct time periods: summer (June to September), winter (October to January), and pre-summer (February to May). The results are compared chronologically within these periods. Additionally, by zoning the Caspian Sea and analyzing the characteristics of the fronts in each region, we provide a spatial comparison of the temperature fronts. This approach allows for a detailed examination of regional variations and patterns in the Caspian Sea's temperature fronts.

3.1. SIED Method

An analysis of the number of temperature fronts detected in the Caspian Sea revealed that the summer period (June to September) had the fewest fronts over the five-year research period. During this time, temperature fronts primarily formed along the coasts of Russia, Kazakhstan, and Turkmenistan, with no fronts observed along the coasts of Iran and Azerbaijan. The fronts that did form during the summer were mostly small and coastal. The largest front during this period, measuring 230 km, changed shape in September 2016. Additionally, a consistent front of about 200 km was observed annually along the Russian coast, and a stable front was noted along the Turkmenistan coast.

The highest number of temperature fronts detected throughout the research period occurred during the winter (October to January). The most and largest fronts were observed in 2018, with the largest front measuring nearly 400 km off the coast of Russia. Generally, fewer fronts formed in October, but their number and size increased in November, December, and January. A relatively large and stable front was consistently present along the coast of Kazakhstan during these months. The Turkmenistan front was one of the most frequent. It sometimes extended from the Garabogazköl Basin to the southern shores of the Caspian Sea, occasionally reaching the coast of Iran, particularly in December. The Azerbaijan fronts typically formed during the warmer months of this period, while the Russian coasts saw fronts of varying numbers and sizes.

During the pre-summer season (February to May), long, coherent, branched, and scattered fronts were occasionally observed. February had the highest number of fronts, with a general decline in front formation as the season progressed. Although most fronts from previous months disappeared during the pre-summer period, some fronts in Kazakhstan, Turkmenistan, and Russia persisted. For example, the Azerbaijan front in 2017 extended from 220 km in January to 400 km in February, reaching the coast of Iran. Fronts detected in March and April were extremely limited, with no significant fronts observed in March 2016 and 2019, except for a few small fronts in the northern Caspian Sea. Figure 2 shows the SIED-detected fronts in the Caspian Sea from December 2015 to 2019.

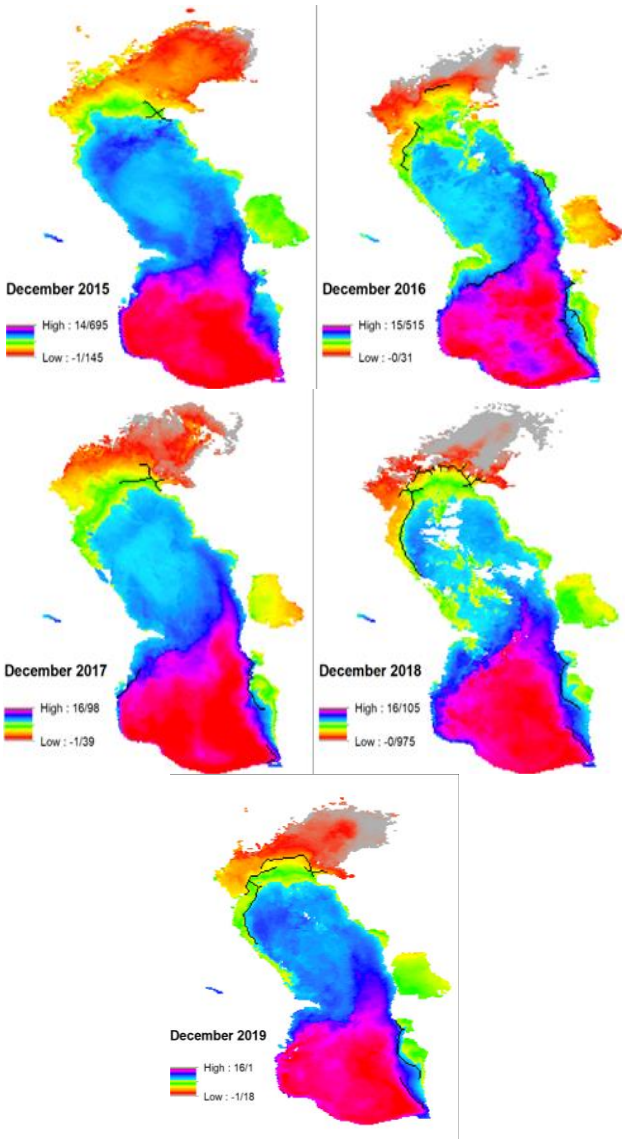

Figure 2. Temperature fronts detected in December from 2015 to 2019

For spatial analysis, the temperature fronts of the Caspian Sea over five years (2015-2019) were identified using the SIED algorithm and divided into five spatial regions, as shown in Figure 3. In Region One, temperature fronts were observed in most months of the study period, except September. In Region Two, temperature fronts remained stable in most months except for February and March. Throughout the five years, fronts were consistently present in the Garabogazköl Basin and Turkmenbashi Gulf in June. September had the fewest temperature fronts across all five regions. In October, temperature fronts began to form gradually, with those in Region Two advancing towards the southern shores of the Caspian Sea. By November, these fronts extended to the coasts of Golestan province in Iran. In January, the fronts became more coherent and moved closer to the coast. During this month, the fronts in Regions Three and Four, which appeared in three of the five years,

extended significantly, with Region Three's front reaching 380 km and Region Four's front reaching 360 km in 2018.

The temperature fronts in Region Four, which were not observed before November, formed this month, reaching a length of 280 km in 2018. Over the years, the fronts in all five regions showed little consistency, being detected mainly in June and July in several years and weakly in August, September, and November. Figure 4 illustrates the monthly temperature fronts extracted using the SIED algorithm across the five regions and years.

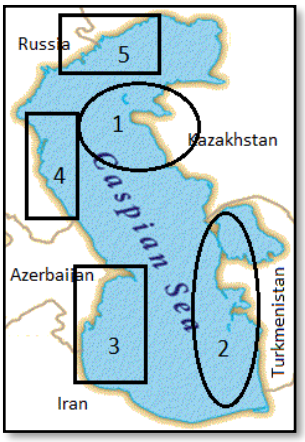

Figure 3. The main regions of stable temperature fronts identified by the SIED algorithm

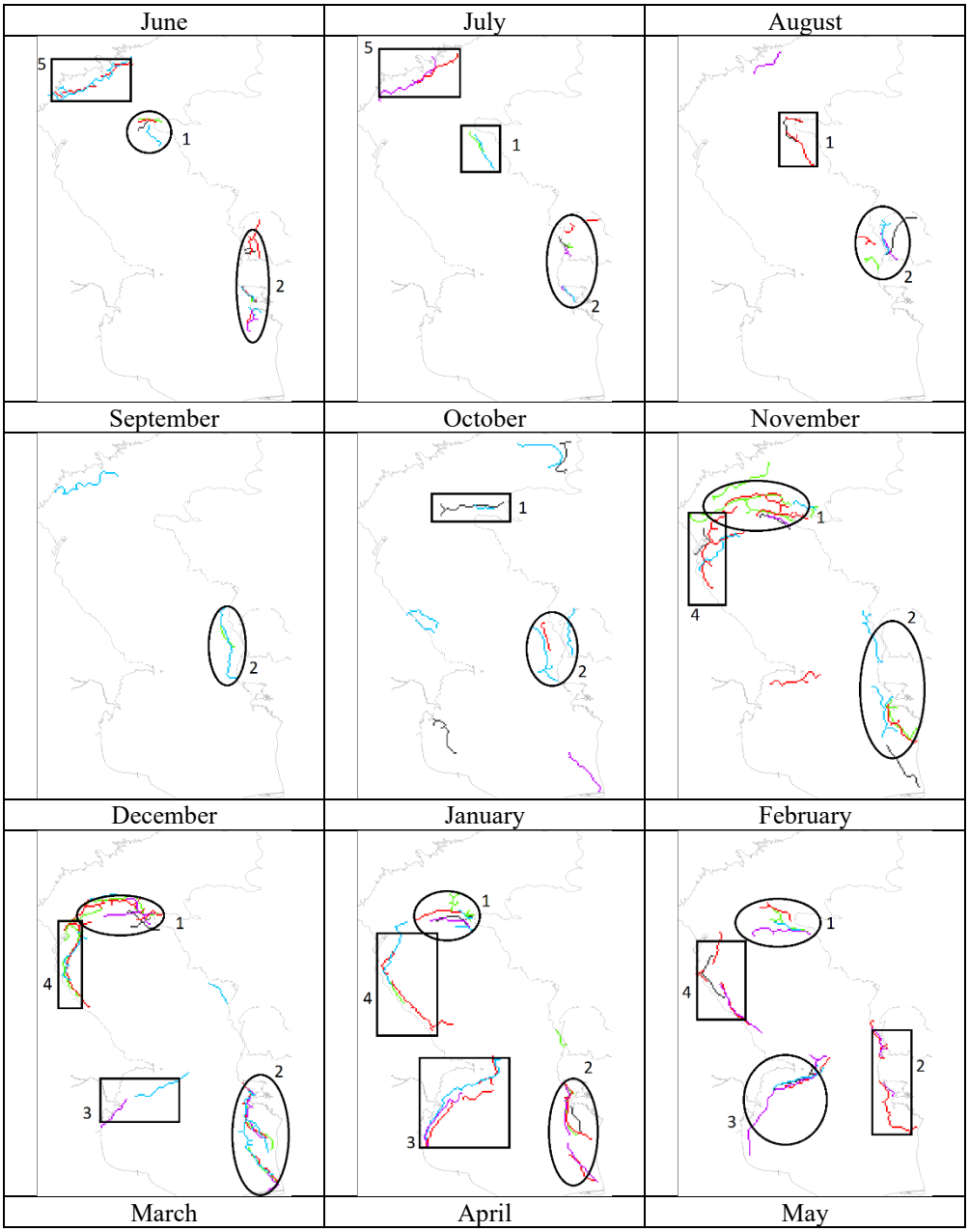

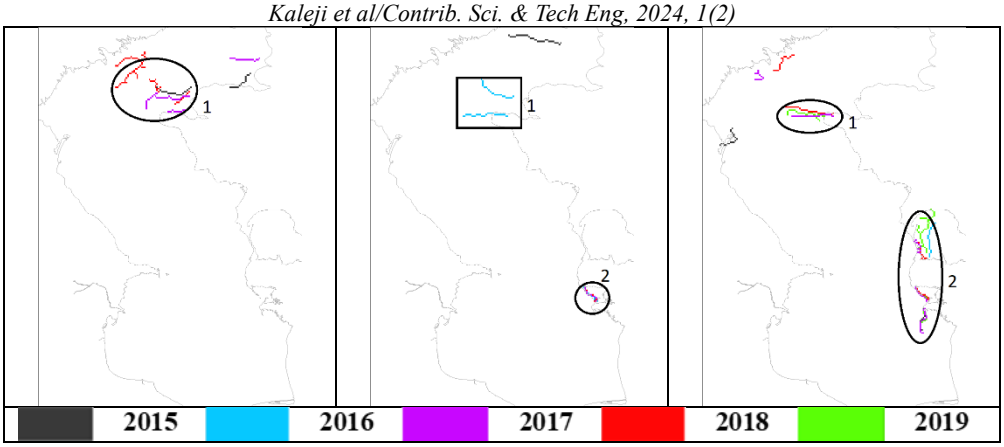

Figure 4. **Monthly interpretation of temperature fronts detected by the SIED algorithm in different years**

3.2. Canny Algorithm

During summer, several temperature fronts were identified using the Canny algorithm. The formation of these fronts was more pronounced in June and July, but their number gradually decreased towards the end of July and September. The fronts formed in the southern Caspian Sea during this period were more coherent and extended towards the coastal areas. In August, most fronts were observed along the coasts of Kazakhstan, Turkmenistan, and Iran, with almost no fronts detected along the coast of Azerbaijan. Although the fronts off the coast of Russia were generally short and scattered, a significant front over 350 km long was detected in September 2017.

In the winter period (October to January), more fronts, mostly in clusters, began to form. Coastal fronts along Kazakhstan and Turkmenistan were consistently detected in October throughout the five-year study period. In November, several fronts formed, but their locations varied. In December 2017, a unique front approximately 300 km long formed 60 km off the coast of Turkmenistan. Similarly, in December 2016, a front about 200 km long was detected 30 km off the coast of Iran (Mazandaran province).

During the pre-summer period (February to May), various types of long, coherent, branched, and discrete fronts were observed. The fronts along the coast of Azerbaijan in February were among the most stable and frequent during the five-year study period. In March, fronts off the coast of Russia were observed consistently, being more coherent in 2015-2016 and more scattered in 2017-2019. Several fronts also formed along the southern shores of the Caspian Sea in May. Figure 5 shows the Canny-detected fronts in the Caspian Sea from November 2015 to 2019.

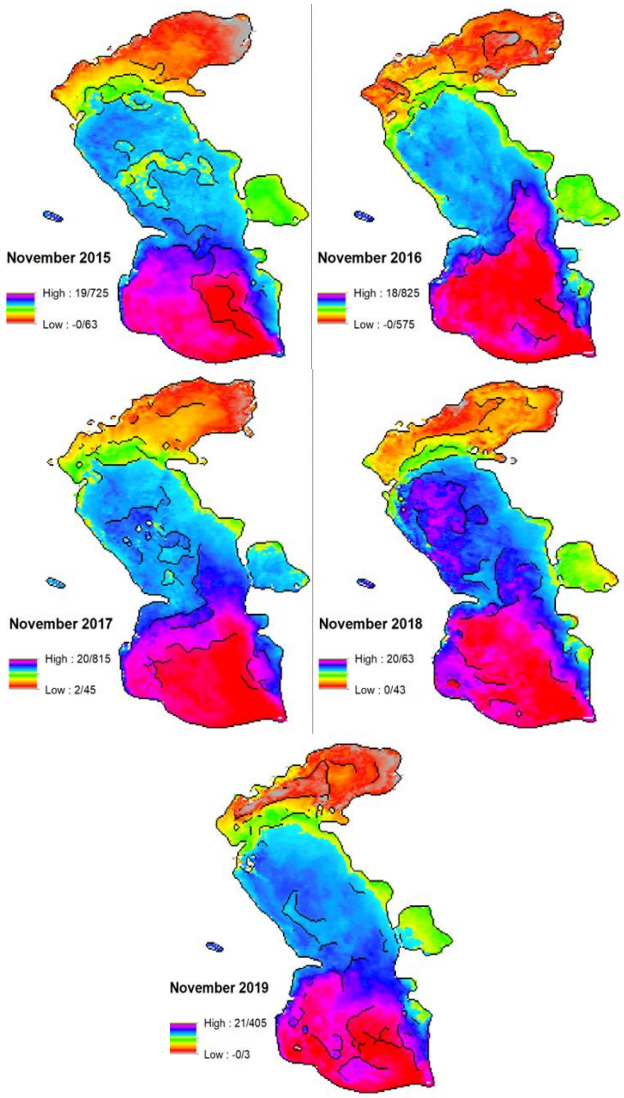

Figure 5. **Sea surface temperature fronts detected by Canny algorithm in November from 2015 to 2019**

The analysis of temperature fronts detected by the Canny algorithm identified six main regions with monthly stable fronts, as shown in Figure 6. In Region 1, temperature fronts form in most months except January, remaining stable as coastal fronts throughout the year. In Region 2, temperature fronts generally do not remain continuous throughout the year; they form in May and persist until December, appearing sporadically. Region 3 only shows a continuous

presence of fronts in March. In Region 4, temperature fronts are detected consistently, except in August. In Region 5, fronts form in September and are consistently observed in October and November. Region 6 exhibits a stable presence of temperature fronts during two three-month periods: September to November and March to May. For the rest of the year, fronts are detected sporadically. Figure 7 illustrates the monthly temperature fronts extracted by the Canny algorithm across the six regions and years.

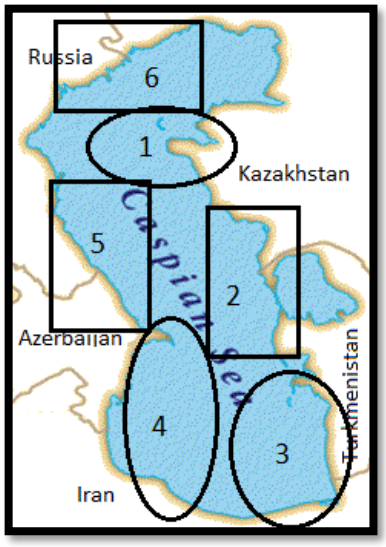

Figure 6. Zoning of sea surface temperature fronts detected by Canny algorithm

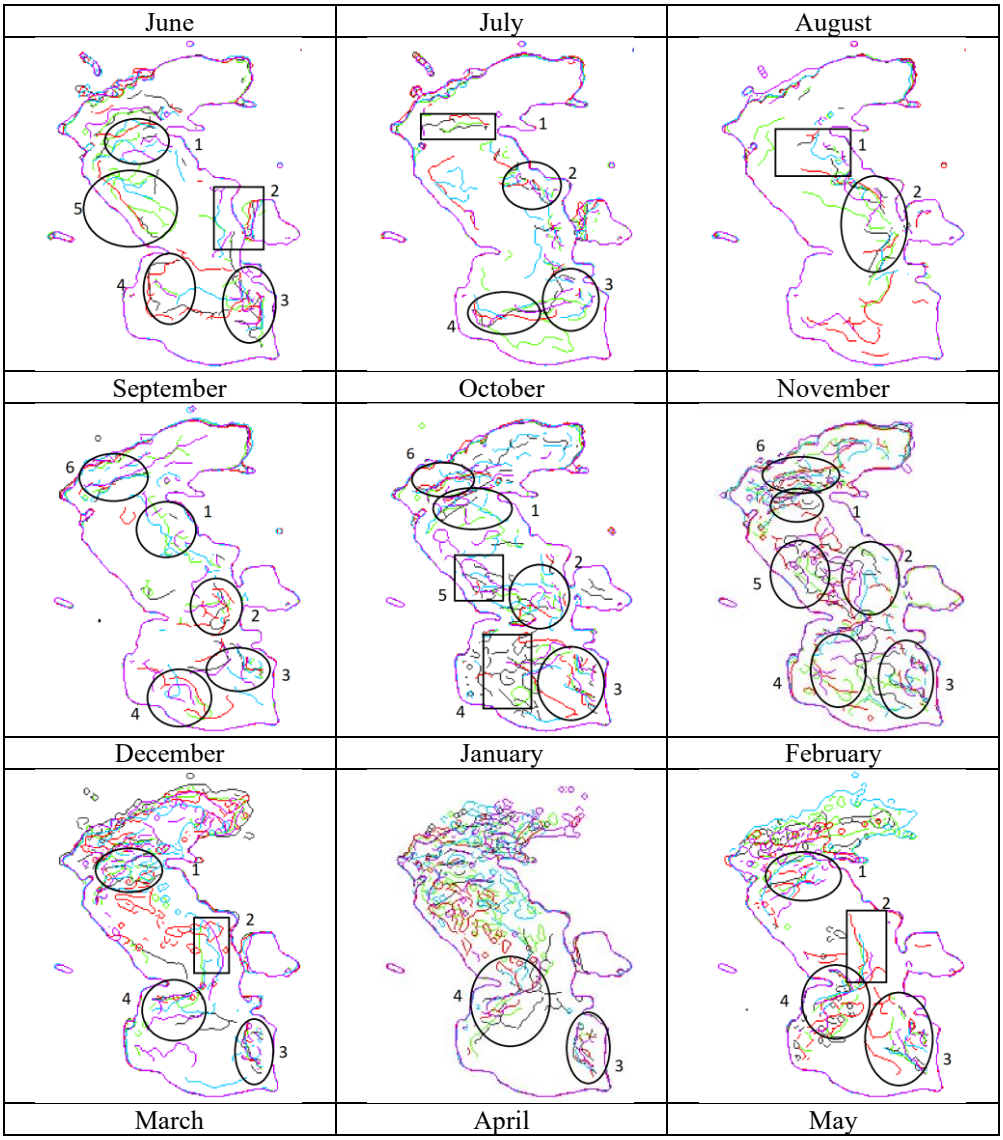

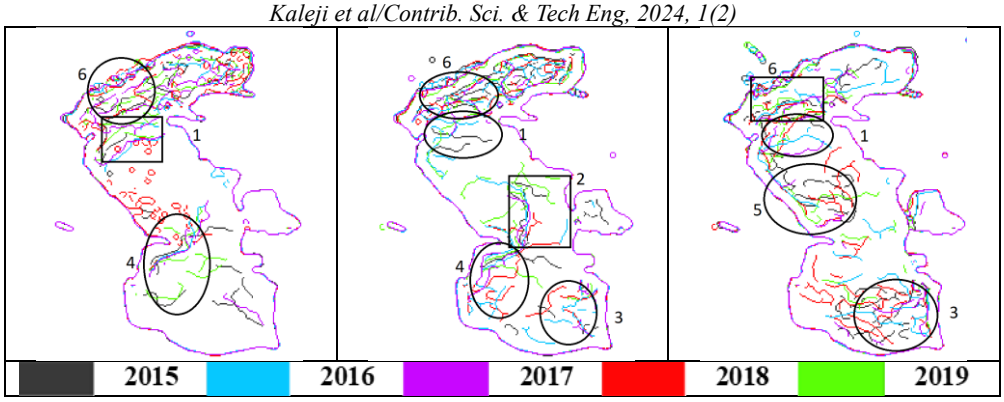

Figure 7. Sea surface temperature fronts separated by year and region

4. Discussion and Results

The SIED algorithm indicated that the lowest presence of stable fronts in the northern half of the Caspian Sea occurs in September and April, while in the southern half, it is in November, March, and April. In contrast, the Canny algorithm showed that the lowest presence of stable fronts in the Caspian Sea is in June, March, and August.

The SIED algorithm revealed that the highest presence of stable fronts in the northern half of the Caspian Sea is in November and December (summer monsoon). In the southern half, it is in January (the last month of the winter monsoon). According to the Canny algorithm, the highest presence of fronts in the Caspian Sea is during the first three months of the winter monsoon. Both algorithms identified a relatively stable front in most months along the eastern coast of the Caspian in the middle and northern regions.

Both algorithms showed significant fronts for the Middle Caspian eastern coasts, particularly near the Garabogazköl Basin and Turkmenbashi Gulf. Relatively stable fronts were detected throughout the year on the eastern coast of the South Caspian. The SIED algorithm revealed unstable but sometimes very long fronts on the western coast of the South Caspian, whereas the Canny algorithm showed stable fronts in this region.

The fronts detected on the eastern coast of the northern half of the Caspian Sea were unstable with both methods and were only present for several months after the warm season. However, the timing of these fronts' formation differed slightly between the two methods. Both algorithms detected the highest presence of fronts during the warm season and very weak and unstable fronts for the rest of the year in the northern regions of the Caspian. The stable presence of fronts lasted longer in the Canny algorithm compared to the SIED algorithm.

Despite differences in the formation time, size, shape, extent, and duration of the fronts identified by the two methods, the general pattern of the fronts was very similar. By comparing the results and examining the time and location of the fronts, it was observed that most fronts identified by both methods occurred in specific areas of the Caspian Sea. One such area is the eastern coast of the Middle Caspian, where the possibility of the upwelling phenomenon is high, according to Mansoury and Sadrinasab [29] and Shiea and Bidokhti [30]. Another area corresponds to the steep regions of the seabed (Figure 1), particularly in the South Caspian, which has the greatest depth changes. Both methods also showed a high number of temperature fronts along the eastern and western coasts of the Middle Caspian, where numerous surface gyres are present [31].

5. Conclusion

By comparing the results obtained from the SIED and Canny methods, it becomes evident that the Canny algorithm detects a significantly higher number of fronts compared to the SIED method. This difference is particularly pronounced in coastal fronts and the southern Caspian fronts. Despite temporal and spatial discrepancies between the fronts detected by these two methods, certain dominant patterns emerge. First, the locations of the largest and strongest fronts identified by both methods largely coincide. Second, the most prominent and intense fronts detected by both methods are aligned with bathymetric lines. Third, both methods consistently revealed significant fronts in the eastern and western regions of the Middle Caspian. Overall, the findings indicate that the Canny algorithm is more effective in identifying local and transient fronts, especially in coastal areas, whereas the SIED method is better suited for detecting dominant and stable fronts.

6. References

[1] Belkin, I. M., Shan, Z., & Cornillon, P. (1998). Global survey of oceanic fronts from Pathfinder SST and in-situ data. Eos Trans. AGU, 79(45).

[2] Zhao, L., Yang, D., Zhong, R., & Yin, X. (2022). Interannual, Seasonal, and Monthly Variability of Sea Surface Temperature Fronts in Offshore China from 1982–2021. Remote Sensing, 14(21), 5336. doi:10.3390/rs14215336.

[3] Ye, Z., & Tozuka, T. (2022). Causal relationship between sea surface temperature and precipitation revealed by information flow. Frontiers in Climate, 4, 1024384. doi:10.3389/fclim.2022.1024384.

[4] Raju, R. M., Nayak, R. K., Mulukutla, S., Mohanty, P. C., Manche, S. S., Seshasai, M. V. R., & Dadhwal, V. K. (2022). Variability of the thermal front and its relationship with Chlorophyll-a in the north Bay of Bengal. Regional Studies in Marine Science, 56, 102700. doi:10.1016/j.rsma.2022.102700.

[5] Timko, P. G., Arbic, B. K., Hyder, P., Richman, J. G., Zamudio, L., O'Dea, E., Wallcraft, A. J., & Shriver, J. F. (2019). Assessment of shelf sea tides and tidal mixing fronts in a global ocean model. Ocean Modelling, 136, 66–84. doi:10.1016/j.ocemod.2019.02.008.

[6] Lan, K. W., Kawamura, H., Lee, M. A., Chang, Y., Chan, J. W., & Liao, C. H. (2009). Summertime sea surface temperature fronts associated with upwelling around the Taiwan Bank. Continental Shelf Research, 29(7), 903–910. doi:10.1016/j.csr.2009.01.015.

[7] Wang, Y., Liu, J., Liu, H., Lin, P., Yuan, Y., & Chai, F. (2021). Seasonal and Interannual Variability in the Sea Surface Temperature Front in the Eastern Pacific Ocean. Journal of Geophysical Research: Oceans, 126(2), 2020 016356. doi:10.1029/2020JC016356.

[8] Xi, J., Wang, Y., Feng, Z., Liu, Y., & Guo, X. (2022). Variability and Intensity of the Sea Surface Temperature Front Associated With the Kuroshio Extension. Frontiers in Marine Science, 9, 9. doi:10.3389/fmars.2022.836469.

[9] Xie, S. P., Hafner, J., Tanimoto, Y., Liu, W. T., Tokinaga, H., & Xu, H. (2002). Bathymetric effect on the winter sea surface temperature and climate of the Yellow and East China Seas. Geophysical Research Letters, 29(24), 81–1–81–4. doi:10.1029/2002GL015884.

[10] Kosarev, A. N. (2005). Physico-Geographical Conditions of the Caspian Sea. The Caspian Sea Environment. The Handbook of Environmental Chemistry, Springer, Berlin, Germany. doi:10.1007/698_5_002.

[11] Kostianoy, A. G., Ginzburg, A. I., Lavrova, O. Y., Lebedev, S. A., Mityagina, M. I., Sheremet, N. A., & Soloviev, D. M. (2019). Comprehensive satellite monitoring of Caspian Sea conditions. Remote sensing of the Asian Seas, Springer, Cham, Switzerland. doi:10.1007/978-3-319-94067-0_28.

[12] Kilpatrick, K. A., Podestá, G., Walsh, S., Williams, E., Halliwell, V., Szczodrak, M., Brown, O. B., Minnett, P. J., & Evans, R. (2015). A decade of sea surface temperature from MODIS. Remote Sensing of Environment, 165, 27–41. doi:10.1016/j.rse.2015.04.023.

[13] Obenour, K. M. (2013). Temporal trends in global sea surface temperature fronts. Master Thesis, University of Rhode Island, Kingston, United States.

[14] Jishad, M., & Agarwal, N. (2022). Thermal Front Detection Using Satellite-Derived Sea Surface Temperature in the Northern Indian Ocean: Evaluation of Gradient-Based and Histogram-Based Methods. Journal of the Indian Society of Remote Sensing, 50(7), 1291–1299. doi:10.1007/s12524-022-01527-6.

[15] Cayula, J. F., & Cornillon, P. (1992). Edge detection algorithm for SST images. Journal of Atmospheric & Oceanic Technology, 9(1), 67–80. doi:10.1175/1520-0426(1992)009<0067:EDAFSI>2.0.CO;2.

[16] Ullman, D. S., & Cornillon, P. C. (2000). Evaluation of front detection for satellite-derived SST data using in situ observations. Journal of Atmospheric and Oceanic Technology, 17(12), 1667–1675. doi:10.1175/1520-0426(2000)017<1667:EOFDMF>2.0.CO;2.

[17] Kahru, M., Håkansson, B., & Rud, O. (1995). Distributions of the sea-surface temperature fronts in the Baltic Sea as derived from satellite imagery. Continental Shelf Research, 15(6), 663–679. doi:10.1016/0278-4343(94)E0030-P.

[18] Nieto, K., Demarcq, H., & McClatchie, S. (2012). Mesoscale frontal structures in the Canary Upwelling System: New front and filament detection algorithms applied to spatial and temporal patterns. Remote Sensing of Environment, 123, 339–346. doi:10.1016/j.rse.2012.03.028.

[19] Blythe, J. N., Da Silva, J. C. B., & Pineda, J. (2011). Nearshore, seasonally persistent fronts in sea surface temperature on Red Sea tropical reefs. ICES Journal of Marine Science, 68(9), 1827–1832. doi:10.1093/icesjms/fsr109.

[20] Ren, S., Zhu, X. U., Drevillon, A., Wang, H., Zhang, Y., Zu, Z., & Li, A. (2021). Detection of sst fronts from a high-resolution model and its preliminary results in the south China sea. Journal of Atmospheric and Oceanic Technology, 38(2), 387–403. doi:10.1175/JTECH-D-20-0118.1.

[21] Karami, H., Akbarinasb, M., & Safarad, T. (2018). Detection coastal thermal fronts in the Persian Gulf and the Oman Sea using MODIS images. Journal of Marine Science and Technology, 17(3), 34-44. (In Persian).

[22] Puthezhath, A. S. (2014). Identification of thermal fronts in the Arabian sea using MODIS-SST data. Master Thesis, Kerala University of Fisheries And Ocean Studies, Ernakulam, India.

[23] Diehl, S. F., Budd, J. W., Ullman, D., & Cayula, J. F. (2002). Geographic window sizes applied to remote sensing sea surface temperature front detection. Journal of Atmospheric and Oceanic Technology, 19(7), 1105–1113. doi:10.1175/1520-0426(2002)019<1105:GWSATR>2.0.CO;2.

[24] Roberts, J. J., Best, B. D., Dunn, D. C., Treml, E. A., & Halpin, P. N. (2010). Marine Geospatial Ecology Tools: An integrated framework for ecological geoprocessing with ArcGIS, Python, R, MATLAB, and C++. Environmental Modelling and Software, 25(10), 1197–1207. doi:10.1016/j.envsoft.2010.03.029.

[25] Tseng, C.-T., Sun, C.-L., Belkin, I. M., Yeh, S.-Z., Kuo, C.-L., & Liu, D.-C. (2014). Sea surface temperature fronts affect distribution of Pacific saury (Cololabis saira) in the Northwestern Pacific Ocean. Deep Sea Research Part II: Topical Studies in Oceanography, 107, 15–21. doi:10.1016/j.dsr2.2014.06.001.

[26] Wall, C. C., Muller-Karger, F. E., Roffer, M. A., Hu, C., Yao, W., & Luther, M. E. (2008). Satellite remote sensing of surface oceanic fronts in coastal waters off west-central Florida. Remote Sensing of Environment, 112(6), 2963–2976. doi:10.1016/j.rse.2008.02.007.

[27] Canny Edge Detection. (2009). Available online: http://opencvexamples.blogspot.com/2013/10/void-canny-

inputarray-image-outputarray.html (accessed on October 2024).

[28] Hrytsyk, V., Medykovskyy, M., & Nazarkevych, M. (2022). Estimation of Symmetry in the Recognition System with Adaptive Application of Filters. Symmetry, 14(5), 903. doi:10.3390/sym14050903.

[29] Mansoury, D., Sadrinasab, M., & Akbarinasab, M. (2018). Seasonal and annual variability in wind fields and circulation of surface waters of the Caspian Sea. Journal of Marine Science and Technology, 17(1), 68-82.

[30] Shiea, M., & Bidokhti, A. A. (2015). The study of upwelling in the eastern coast of the Caspian Sea using numerical simulation. Journal of the Earth and Space Physics, 41(3), 535–545.

[31] Lavrova, O., & Mityagina, M. (2017). Satellite survey of internal waves in the Black and Caspian Seas. Remote Sensing, 9(9), 892. doi:10.3390/rs9090892.